2000PASJ...52.1037I

PASJ: Publ. Astron. Soc. Japan **52**, 1037–1044 (2000)

Multi-Frequency VLBI Observations of OT 081

Satoru IGUCHI,[1,2] Kenta FUJISAWA,[2] Seiji KAMENO,[2] Makoto INOUE[2],
Zhi-Qiang SHEN,[2] Kouichi HIROTANI,[2] and Makoto MIYOSHI[2]

[1]*Department of Electronic Engineering, University of Electro-Communications, Choufu, Tokyo 182-8585*
E-mail (SI): iguchi@hotaka.mtk.nao.ac.jp
[2]*National Astronomical Observatory, Mitaka, Tokyo 181-8588*

(Received 2000 January 25; accepted 2000 September 28)

Abstract

We have observed OT 081 at 4.8, 8.4, 15, and 22 GHz, with the VLBI Space Observatory Programme (VSOP) and the Very-Long-Baseline Array (VLBA) after its radio burst on 1998 May. Multi-frequency VLBI images show a dominant component D and a weak component C1, which is a knot of the jet extending to the north-west direction. The derived physical parameters of component D are the Doppler factor, $\delta_{\rm eq} \sim 32.0$, the Lorentz factor of $16.0 < \Gamma < 16.9$, and the viewing angle, $\phi < 0\overset{\circ}{.}68$. It appears that although $\delta_{\rm eq}$ of component C1 is smaller than that of componet D by one order of magnitude, Γ of component C1 is about twice the range as that of component D at the 1 σ level. However, ϕ of component D is different from that of component C1. The rapid variability of the flux density of OT 081 is suggested to be due to the variation of ϕ.

Key words: BL Lacertae objects: individual (OT 081 = 1749+096) — galaxies: active — radio sources: variable — techniques: interferometric

1. Introduction

BL Lacertae objects are characterized by their flat spectrum, high variability in their light curve, and high polarization degree (Miller et al. 1978). Bright continuum emission compared with narrow lines is thought to be a Doppler-boosting effect for synchrotron emission in relativistic jets (see, e.g., Urry, Padovani 1995). OT 081 ($z = 0.322$) is an ultralumious BL Lacertae object with strongly broad-band variability in the X-ray (Urry et al. 1996), optical (Clements et al. 1995), mm- and cm- radio regimes [Reuter et al. 1997; Teräsranta et al. 1998; University of Michigan Radio Astronomy Observatory (UMRAO) database (http://www.astro.lsa.umich.edu/obs/radiotel/umrao.html)].

OT 081 became active in the 1990s and has experienced bursts with intervals from 1 to 3 years at the radio regume (Reuter et al. 1997; Teräsranta et al. 1998; UMRAO database). For investigating the origin of the radio variability, we observed this source at 4.8, 8.4, 15, and 22 GHz with the VLBI Space Observatory Programme (VSOP) (Hirabayashi et al. 1998) and the Very-Long-Baseline Array (VLBA) (Napier et al. 1994) after its radio burst in 1998 May. We present here multi-frequency VLBI images of OT 081, and discuss the properties of each component, the jet structure in this source, and the possible origin of its variability.

We adopt a Hubble constant (H_0) of 100 h km s^{-1} Mpc^{-1} and a deceleration parameter (q_0) of 0.5. These give a luminosity distance to OT 081 of $D_{\rm L} = 1.03\ h^{-1}$ Gpc. An angular size or separation of 1 mas then corresponds to 2.87 h^{-1} pc. A proper motion of 1 mas yr^{-1} corresponds into a speed of $\beta_{\rm app} = 12.4\ h^{-1}$. We use the following definition of the spectral index: $S \propto \nu^{\alpha}$.

2. VLBI Observations and Data Reduction

OT 081 was observed at 4.8 GHz with the VSOP satellite HALCA for 4.0 hr, and with the VLBA array (except St. Croix, Brewster, and Los Alamos) for 7.5 hr on 1998 August 20. The data were recorded in the VLBA format, using two intermediate frequency (IF) bands with an observing bandwidth of 16 MHz. Data from the HALCA was downlinked to the Satellite Tracking Station (STS) at a bit rate of 128 Mbps. The observing data were cross-correlated with the VLBA correlator at Socorro, having 128 spectral channels at each IF. Fringe visibilities were detected at full time in the HALCA data recorded at the STS in Robledo (Spain), and for 90 min in that of Goldstone (USA).

VLBA observations were made at sky frequencies of 8.4, 15, and 22 GHz with the full VLBA array on 1998 November 7. The observing times at each frequency were 30, 20, and 30 min, respectively. The data were

© Astronomical Society of Japan • Provided by the NASA Astrophysics Data System

2000PASJ...52.1037I

recorded in the VLBA format, using four IF bands with an observing bandwidth of 8 MHz, each having 256 spectral channels. The observed data were cross-correlated with the VLBA correlator at Socorro.

2.1. *Fringe Fitting*

The correlated data include the residual delays and delay rates due to estimating errors of the satellite orbit, and to fluctuations of the path length of the atmosphere and the ionosphere, etc. The residuals show a phase slope over an entire band from 0 Hz to the band edge. The phase slope was corrected with a calibration method, called fringe fitting. The fringe fitting was performed using the Astronomical Image Processing System (AIPS) developed by the National Radio Astronomy Observatory.

For the VSOP, we used solution intervals of 1 min, and accepted all solutions with SNR > 7. After the fringe fitting, the residual phase variations were found to be within $1\overset{\circ}{.}5$ on the ground baselines, and $< 10^\circ$ on the HALCA baselines. Under inspecting phase and amplitude responses in the IF bandpasses, the last 43 channels were flagged out in each IF. This means that the 85 channels were used in each IF, so that the total observing bandwidth was reduced to 21.25 MHz.

For the VLBA, fringe fitting was also undertaken using AIPS. After inspecting the IF bandpasses, the last 56 channels were flagged in each IF, owing to a significant (50–80%) amplitude loss. This means that because 200 channels were used in each IF, the total observing bandwidth was reduced to 25 MHz.

2.2. *Amplitude Calibration*

In the VLBI, an a-priori amplitude calibration was applied to derive the fringe visibility from the correlated data. The a-priori amplitude calibration was based on system-temperature measurements and elevation-dependent antenna gain curves. We further used another reduction method, the UVCROSS task installed in the Caltech VLBI Package (Pearson 1991), to accurately calibrate the relative fringe amplitude between all radio telescopes. This method corrects the amplitude using crossing points in the *uv* coverage (figure 1). We next used the total flux density referred from the UMRAO database to accurately calibrate the absolute fringe amplitude. In addition, a correction for atomospheric opacity effects was applied at 15 and 22 GHz using the APCAL task in AIPS. The accuracy of the amplitude calibration was determined from a comparison of the raw-calibrated data with the self-calibrated data sets obtained for the program and the calibrator sources during the imaging and model fitting. On this basis we can confidently assign an uncertainly in the amplitude calibration of $\sim$ 1–15% at 4.8, 8.4, and 15 GHz and $\sim$ 5–20% at 22 GHz.

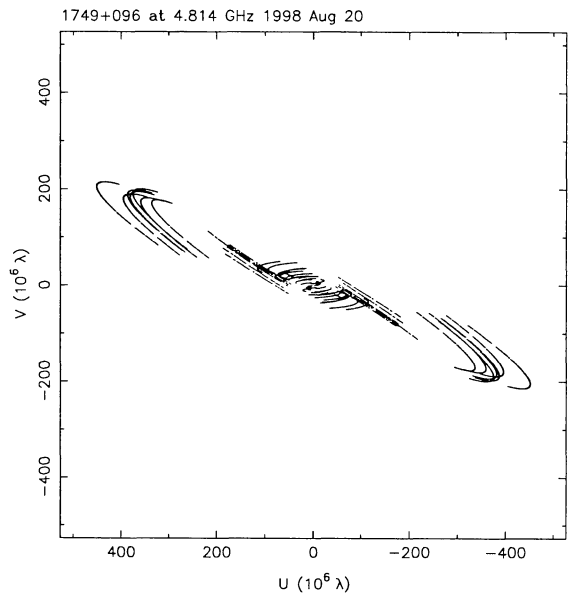

Fig. 1. *uv*-coverage of the VSOP observation of OT 081. The inner ellipses represent the baselines between the VLBA telescopes; the space baselines are grouped into larger ellipses extending at P.A.= 65°.

2.3. *Imaging*

The visibility data were exported into DIFMAP (Shepherd et al. 1994) and further time-averaged into 30-s bins. The data were analyzed for structural information with the DIFMAP. Images were made using the "clean mapping" and "self-calibration" techniques. Figure 2 shows the final images with VSOP at 4.8 GHz, and with VLBA at 8.4, 15, and 22 GHz, respectively. For a quantitative analysis of the structure information in the images, we applied model fitting with several Gaussian components given by the IMFIT task in AIPS. All images were fitted by two componets: a dominant component D, and a weak component C1, which is a knot of the jet extending to north-west direction. The derived parameters are listed in table 1: the flux density (S_ν), the relative Right Ascension position ($\tau_{\rm ra}$), the relative Declination position ($\tau_{\rm dec}$), the major-axis size ($\tau_{\rm ma}$), the minor-axis size ($\tau_{\rm mi}$), and the position angle ($\phi_{\rm p}$). Note that model parameters are often correlated, e.g., the flux density and the angular size of very extended components.

3. Results

3.1. *Spectral Fitting*

The spectral information for an individual component is limited by the frequency coverage and the quality of the VLBI measurements near a given epoch. From the UMRAO database, the total flux density of OT 081 at 4.8 GHz was 2.31 ± 0.02 Jy at the epoch of the VSOP ob-

© Astronomical Society of Japan • Provided by the NASA Astrophysics Data System

2000PASJ...52.1037I

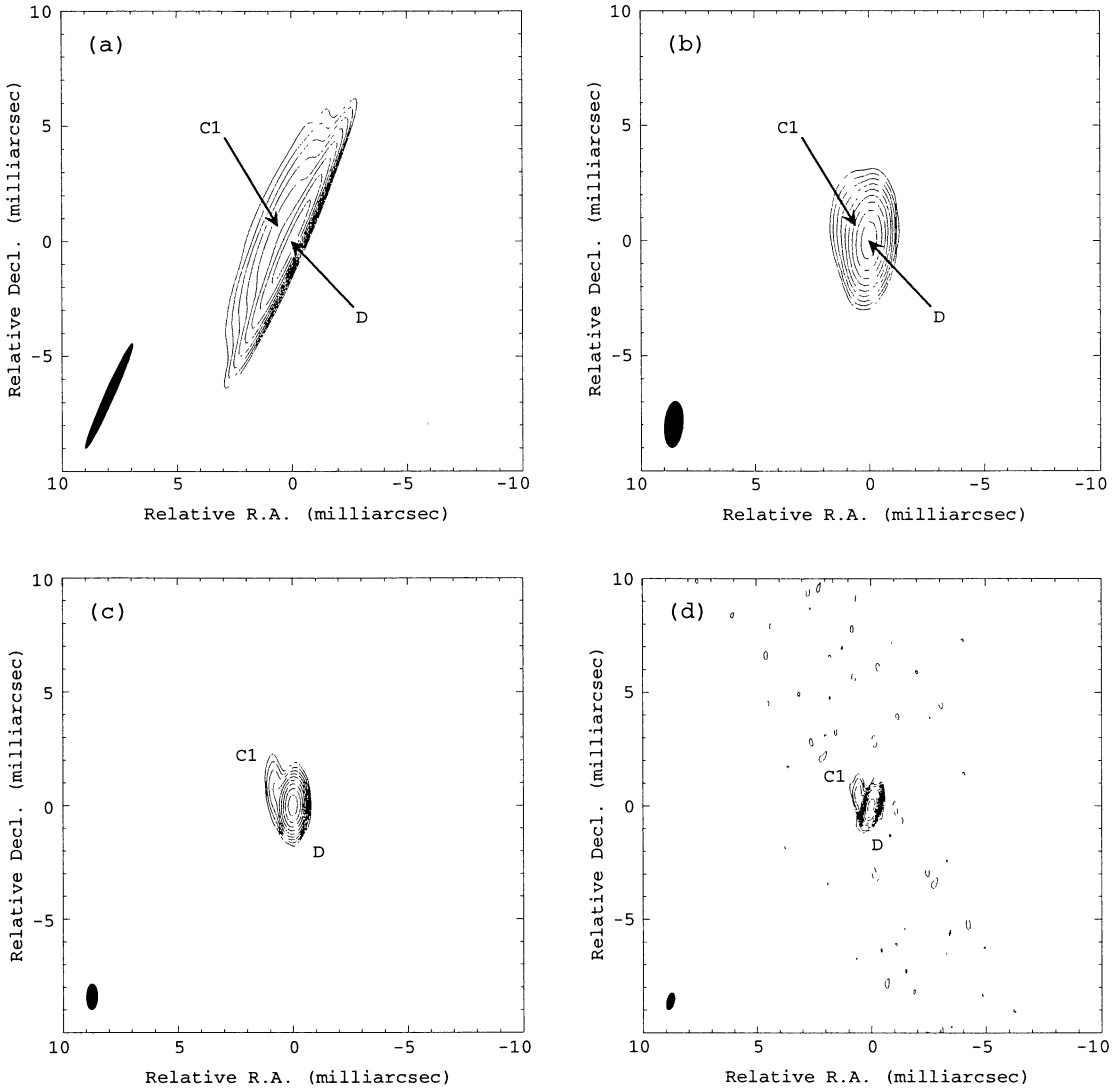

Fig. 2. Four images of OT 081 at 4.8, 8.4, 15, and 22 GHz, respectively. The map contours are at (−0.25, 0.25, 0.5, 1.0, 2.0, 4.0, 8.0, 16.0, 32.0, 64.0%) $\times P$, where P is the peak flux density. Map (a) was made at 4.8 GHz with the VSOP, and P is 1.56 Jy/beam with a restoring beam of 5.00 mas×0.413 mas at P.A.= $-24\overset{\circ}{.}2$; Map (b) was made at 8.4 GHz with the VLBA, and P is 4.32 Jy/beam with a restoring beam of 2.04 mas×0.822 mas at P.A.= $-5\overset{\circ}{.}56$; Map (c) was made at 15 GHz with the VLBA, and P is 4.58 Jy/beam with a restoring beam of 1.15 mas×0.492 mas at P.A.= $-1\overset{\circ}{.}1$; Map (d) was made at 22 GHz with the VLBA, and P is 4.89 Jy/beam with a restoring beam of 0.783 mas×0.329 mas at P.A.= $-13\overset{\circ}{.}0$.

servation (1998 August 20), whereas it was 3.15 ± 0.10 Jy at the epoch of VLBA observation (1998 November 7). This means that the flux density of OT 081 increased by 0.84 ± 0.12 Jy during the two observing epochs. We corrected this variability of the flux density in figure 3 as follows. The total flux density of OT 081 is dominated by component D (table 1). Moreover, we can confirm that the flux densities of several components, except for component D, at 2.3 and 8.4 GHz had not almost increased within one year (Fey et al. 1996b; Fey, Charlot 1997). We have assumed that the radio variability of OT 081 depends on component D. Thus, we corrected the flux density of component D at 4.8 GHz from 1.530 Jy to 2.37 Jy (i.e., +0.84 Jy), as shown in figure 3.

The 2.3 GHz flux density was estimated from our 2.3 GHz VLBA image (1998 December 15). The variability of the flux density at 2.3 GHz was weak for a period of several months (Waltman et al. 1991; Fey et al. 1996b; Fey, Charlot 1997). The monitor VLBI observations show that the variability of 2.3 GHz became about 10% within two months since 1997 July (Fey et al. 1996b; Fey, Charlot 1997). Therefore, we did not apply

© Astronomical Society of Japan • Provided by the NASA Astrophysics Data System

2000PASJ...52.1037I

Table 1. Parameters of the Gaussian componets.

Component (1)	S_ν [Jy] (2)	τ_{ra} [mas] (3)	τ_{dec} [mas] (4)	τ_{ma} [mas] (5)	τ_{mi} [mas] (6)	ϕ [degree] (7)
Frequency 4.8 GHz (VSOP: 1998 August 20)						
D	1.530±0.011	0.000	0.000	0.684±0.009	0.141±0.001	−25.07±0.12
C1	0.656±0.032	0.423±0.002	0.301±0.005	1.422±0.019	0.423±0.051	18.325±1.203
Frequency 8.4 GHz (VLBA: 1998 November 7)						
D	4.381±0.010	0.00	0.00	0.218±0.003	0.110±0.002	−26.36±0.98
C1	0.261±0.020	0.672±0.002	0.654±0.004	1.084±0.014	0.345±0.014	12.58±0.78
Frequency 15 GHz (VLBA: 1998 November 7)						
D	4.837±0.023	0.00	0.00	0.238±0.001	0.076±0.002	−28.98±0.43
C1	0.166±0.024	0.787±0.003	0.678±0.010	1.344±0.023	0.202±0.050	10.52±0.59
Frequency 22 GHz (VLBA: 1998 November 7)						
D	5.150±0.032	0.00	0.00	0.233±0.001	0.065±0.002	−33.57±0.29
C1	0.137±0.035	0.545±0.004	0.444±0.012	1.511±0.019	0.398±0.049	8.23±0.82

Note. Column 1 gives the component identification, column 2 gives its flux density (S_ν), columns 3 and 4 give the Right Ascension and Declination of the positions relative to component D, columns 5, 6, and 7 give the major-axis size (τ_{ma}), the minor-axis size (τ_{mi}), and the position angle of major axis (ϕ_p), respectively. The IMFIT task varies parameters of interest and examines the resultant $\Delta\chi^2$. The errors of models fitting are formal 1 σ values. The errors are given by IMFIT and contain amplitude calibration uncertainties.

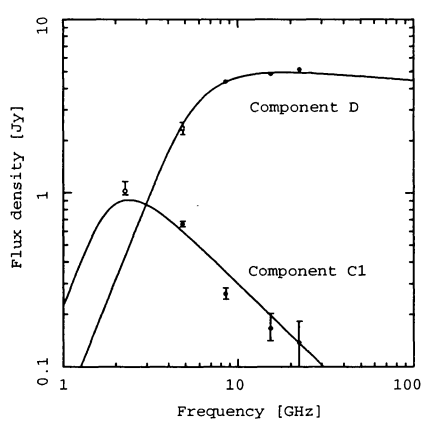

Fig. 3. Radio spectra of OT 081 on 1998 November 7. The flux density of the unresolved component is given by the open circle, the flux density of each components is given by the filled circles, and the corrected flux density of component D is given by the open square. The epoch of observation was as follows: 2.3 GHz (1998 December 15), 4.8 GHz (C1: 1998 August 20, D: 1998 November 7), 8.0 GHz (1998 November 7), 15 GHz (1998 November 7), 22 GHz (1998 November 7).

any correction to the flux density at 2.3 GHz to do the spectra fitting. Because the 2.3 GHz VLBA observation could not resolve between components C1 and D (Fey et al. 1996a), the net flux density is given by the open circle plotted at 2.3 GHz in figure 3.

For a plasma with electron self-absorption, the spectral distribution of emission is (Pacholczyk 1970):

$$S_\nu \propto \left(\frac{\nu}{\nu_d}\right)^{\alpha_t} \left\{1 - \exp\left[-\left(\frac{\nu_d}{\nu}\right)^{\alpha_t - \alpha}\right]\right\}, \quad (1)$$

where ν_d is the frequency at which the optical depth, (τ_s) is 1, and α_t and α are the spectral indices of the optically thick and optically thin parts of the spectrum, respectively. For a plasma with a homogeneous synchrotron spectrum, α_t is 2.5. We used this synchrotron self-absorption model for the spectra fitting (figure 3).

The physical parameters of component D are as follows: the optical-thin spectral index (α) is -0.08 ± 0.01, the peak frequency (ν_m) is 15.8 ± 1.0 GHz, and the peak flux density (S_m) is 5.00 ± 0.03 Jy. Those of component C1 are as follows: the optical-thin spectral index (α) is -0.98 ± 0.05, the peak frequency (ν_m) is 2.37 ± 0.30 GHz, and the peak flux density (S_m) is 0.90 ± 0.09 Jy. These parameters of each component are listed in table 2.

© Astronomical Society of Japan • Provided by the NASA Astrophysics Data System

2000PASJ...52.1037I

Table 2. Physical Parameters of the OT 081 ($h = 0.75$).

Component	D	C1
α	-0.08 ± 0.01	-0.98 ± 0.05
$\nu_{\rm m}$ [GHz]	15.8 ± 1.0	2.37 ± 0.30
$S_{\rm m}$ [Jy]	5.00 ± 0.05	0.90 ± 0.09
$\beta_{\rm app}$	$<7.58\pm0.49$	11.2 ± 2.3
$\theta_{\rm d}$ [mas]	0.222 ± 0.003	1.396 ± 0.059
$\delta_{\rm eq}$	$32.0\pm^{6.0}_{4.8}$	$2.46\pm^{0.88}_{0.57}$
Γ	$16.0\pm^{3.0}_{2.4} < \Gamma < 16.9\pm^{2.8}_{2.2}$	$19.9\pm^{11.4}_{7.7}$
ϕ	$< 0.^\circ68\pm^{0.26}_{0.20}$	$8.^\circ93\pm^{1.84}_{1.25}$

Note. These values are quoted from a single epoch (1998 November 7). However, $\beta_{\rm app}$ of C1 was derived from combining multiple epochs (see figure 4).

3.2. *Apparent Speed*

Our two VLBI images at 15 GHz on 1998 November 7 (figure 4) and December 15 show that component C1 is extending to the north-west direction (position angle is about 40°). The other five images were obtained from past VLBA observations (Kellermann et al. 1998; Fey et al. 1996a; Fey, Charlot 1997). The radio bursts of OT 081 occurred in 1995 January, 1997 May, and 1998 May (figure 5). The OT 081 image on 1997 August 28 shows that this source was single and compact after the radio burst on 1997 May. Our two images (1998 November 7 and December 15) after the radio burst in 1998 May show the separation between each component was almost the same during each epoch. Hence, we suppose that component C1 was created at the radio burst in 1997 May. We measured the proper motion of 0.68 ± 0.14 mas yr^{-1} for component C1 with the respect to D using the three images (1997 August 28, 1998 November 7, and December 15). We then fitted three positions with a straight line, because only three data are not sufficient for a polynomial fitting.

We also give an upper limit on the speed of the structure change of component D using its size and the burst epoch. Our VLBA images (figure 2) show that component D has three interesting properties. First, the higher the observing frequency is, the smaller the minor-axis size is (figure 6). Next, in all frequencies, the position angle of major axis is almost constant ($-30°$; see table 1). Finally, the major-axis size does not depend on the observing frequency, and is almost constant at all frequencies (average $\tau_{\rm ma} = 0.230 \pm 0.015$ mas). These properties are simply interpreted by saying that component D probably has unresolved jets extending in the direction parallel to the major axis, and that the real size of component D is represented by the width in the direction perpendicular to the jet axis, i.e., the major axis. The knot components created at the radio burst in 1998 May have not been identified (figure 5). If the major-axis size of 0.230 ± 0.015 mas is created by this burst, the upper limit of the proper motion of component D would be $< 0.46\pm0.03$ mas yr^{-1}. Note that the major axis quoted for component D is close

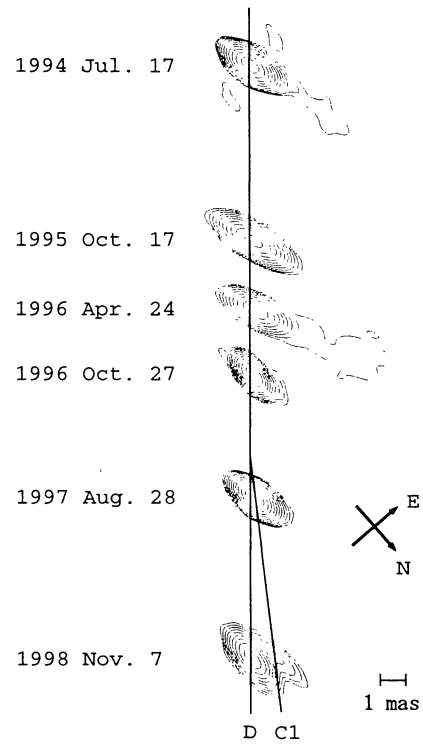

Fig. 4. Proper motion of the knot components in OT 081. The six images were observed at 15 GHz with VLBA.

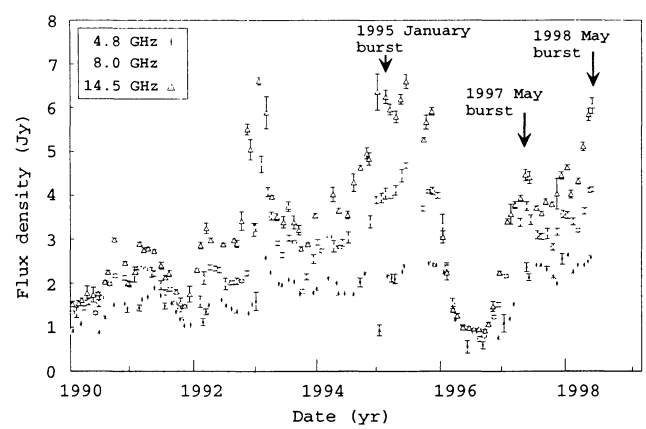

Fig. 5. Light curves of OT 081 at 4.8 GHz (crosses), 8.0 GHz (open circles), and 14.5 GHz (filled triangles) for a period of about 9 yr from the UMRAO database. The errors are almost less than 0.2 Jy at each frequency.

© Astronomical Society of Japan • Provided by the NASA Astrophysics Data System

2000PASJ...52.1037I

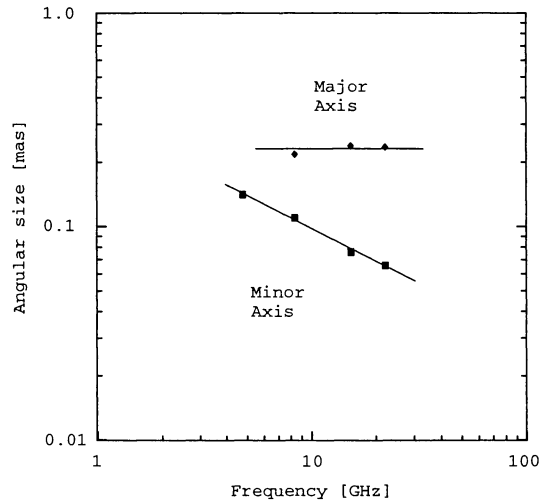

Fig. 6. Relative size of the major-axis and the minor -axis for component D. The plotted data were obtained from table 1. The major-axis size of component D is almost constant at all frequencies, where the 4.8 GHz VSOP data is rejected in this discussion because our 4.8 GHz image has a low-resolution beam parallel to the major axis (figure 1).

to the position angle of the beam at all frequencies, and its size is much smaller than the FWHM of the beam. On the other hand, Lobanov et al. (1999) showed three knots in the direction of P.A. $\sim 0°$ within 0.4 mas from a 86-GHz VLBI observation of OT 081 in 1993. We believe that the major-axis size derived in this paper is the upper-limit size of the unresolved component D.

The resultant values of the apparent speed, $\beta_{\rm app}$, of each component are listed in table 2 (assumed $h = 0.75$).

3.3. Estimation of Equipartition Doppler Factor

We assume that each component is homogeneous, containing an isotropic power-law distribution of relativistic electrons, $N(E)dE = N_0 E^{-p} dE$, and a tangled magnetic field B. The component moves with the Lorentz factor, $\Gamma = (1-\beta^2)^{-1/2}$, at an angle ϕ to the line of sight, giving a Doppler factor of $\delta = \Gamma^{-1}(1-\beta\cos\phi)^{-1}$. A terrestrial observer measures the peak flux density, $S_{\rm m} = S^*_{\rm m}[(1+z)/\delta]^{-3}$, at frequency $\nu_{\rm m} = \nu^*_{\rm m}[(1+z)/\delta]^{-1}$, where the quantities with asterisk are the peak values that would be measured by a co-moving observer. The variability of the observed flux density depends on the variations in the intrinsic peak flux density $S^*_{\rm m}$, Γ, and ϕ.

Since the 22 GHz VLBA image has the highest resolution among our VLBI images, we adopted 0.233 mas×0.065 mas and 1.511 mas×0.398 mas as the size of components D and C1, respectively. The angular diameter of a given component, obtained by modeling it as a sphere, is greater than the observed angular diameter, $\theta_{\rm FWHM} = \sqrt{\tau_{\rm ma}\tau_{\rm mi}}$ which is the geometric mean of the component size. Marscher (1987) proposed a connection for this by using $\theta_{\rm d} = 1.8\ \theta_{\rm FWHM}$ for an optically thin sphere. The angular diameters, $\theta_{\rm d}$, of each component are listed in table 2.

We derived an equipartition Doppler factor of each component using an equipartition model, which is based on the assumption of energy equipartition between the magnetic field and the particles (Readhead 1994):

$$\delta_{\rm eq} = \left\{ [10^3 F(\alpha)]^{34} \left[\frac{2h}{1-(1+z)^{-\frac{1}{2}}} \right]^2 \times (1+z)^{15-2\alpha} S_{\rm m}^{16} \theta_{\rm d}^{-34} (10^3 \nu_{\rm m})^{-35-2\alpha} \right\}^{\frac{1}{13-2\alpha}}. \tag{2}$$

The numerical function, $F(\alpha)$, is given in Scott and Readhead (1977). The resultant values of $\delta_{\rm eq}$ of each component computed from $\theta_{\rm d}$, $S_{\rm m}$, $\nu_{\rm m}$, and α, are listed in table 2.

3.4. Estimations of Lorentz Factor and Viewing Angle

The Lorentz factor (Γ) and the viewing angle (ϕ) are calculated with the equipartition Doppler factor ($\delta_{\rm eq}$) and the apparent speed ($\beta_{\rm app}$). The Lorentz factor is written as

$$\Gamma = \frac{\beta_{\rm app}^2 + \delta^2 + 1}{2\delta}, \tag{3}$$

and the viewing angle is

$$\phi = \tan^{-1}\left(\frac{2\beta_{\rm app}}{\beta_{\rm app}^2 + \delta^2 - 1} \right). \tag{4}$$

[equations (B5) and (B7) in Ghisellini et al. (1993)]. Instead of substituting $\delta = \delta_{\rm eq}$, we can actually compute these factors. There is much justification in adopting the equipartition Doppler factor ($\delta_{\rm eq}$). As Güijosa and Daly (1996) pointied out, the $\delta_{\rm eq}$'s of various AGN jets have a high correlation with $\delta_{\rm min}$, the minimum allowed Doppler factor derived by comparing the predicted and observed self-Compton fluxes (Marcher 1987).

We obtained only the upper limit of $\beta_{\rm app}$ for component D (see subsection 3.2). Then, the upper limits of ϕ and Γ were derived using $\delta_{\rm eq}$ and $\beta_{\rm app}$. Also, the lower limit of Γ was derived without $\beta_{\rm app}$. The resultant values of Γ and ϕ of each component are listed in table 2.

4. Discussion

4.1. Relations between the Flux Variability and the Doppler Factor

Table 2 shows that the variations of $\delta_{\rm eq}$ and $\beta_{\rm app}$ are contributed weakly by the variation of Γ from 16 to 20

© Astronomical Society of Japan • Provided by the NASA Astrophysics Data System

2000PASJ...52.1037I

and strongly by the variation of ϕ from 0.°68 to 8.°93. It appears that Γ of component D corresponds to that of component C1 within a factor of 2, while the ϕ of component D is different from that of component C1. Hence, the difference of $\delta_{\rm eq}$ between each component by one order of magnitude is influenced by the variation of ϕ. The strongly variable flux density of OT 081 could be attributed to this variation of ϕ, as shown below.

The variability of the observed flux density depends on the variations of $S^*_{\rm m}$ and δ. Basically, a radio burst occurs first at high frequency and then shifts to low frequency. The monitoring data of 4.8, 8.0, and 14.5 GHz from the UMRAO database show a big drop in 1996–1997 simultaneously at all three frequencies (figure 5). This rapid drop event could be interpreted as a variation of δ ($=\delta_{\rm eq}$). Especially, in the case of OT 081, δ is strongly determined by ϕ.

The scattering event by a galactic region of high electron-density turbulence, which has an angular extent comparable to that of OT 081, has been reported by Fey et al. (1996a). The scattering event shows different variations in the radio light curves at each observing frequency. The drop event in OT 081, however, does not depend on the observing frequencies, suggesting that the scattering matter does not cause the drop event.

The flux density of OT 081 from 1995 to 1997 changed by a factor of at least 8 at 14.5 GHz (figure 5). Our multi-frequency images showed that the flux density of each component in OT 081 is strongly related to the variation of δ ($=\delta_{\rm eq}$) as we have shown in section 3. Therefore, the variability of flux density could be interpreted by changing δ by a factor of 2. For the case that only the variation of Γ contributes to the variation of δ, one requires changing Γ from 16.9 to 8.5. If only ϕ varies, the variation of δ requires changing ϕ from 0.°68 to 3°. The derived variation angle of 3° is smaller than ϕ of component C1, which is 8.°93, while the variation of Γ between each component is from 16 to 20. Our result shows that the rapid variability of the flux density of OT 081 could be due to the variation of ϕ.

Note that there is a possibility that δ and Γ of component D are stronger than that of our estimations, bacause we can not accurately measure the major-axis size and the apparent speed for component D. Hence, higher resolution VLBI observations are necessary to clarify the relation between the variability and ϕ.

4.2. Component D

The derived optically thin spectral index of D is very flat, and would imply an electron energy distribution that is extremely unusual. We believe that component D consists of several components, shown as the 86-GHz VLBI image (Lobanov et al. 1999). A 86-GHz CMVA (Coordinated Millimeter VLBI Array) observation can achieve an angular resolution of 0.05 mas, which is smaller than the minor-axis size of component D (0.065 mas). The highest-resolution observation has a possibility of resolving the structure extending in the direction parallel to the major-axis of component D. We have already proposed an 86-GHz CMVA observaton to study the extremely Doppler-boosting jets. This observation would also be effective to clarify the structure of the inner jets in BL Lac objects. Especially, it will be important to accurately derive the Doppler and Lorentz factors.

5. Summary

Our work has yielded significant results on the spectral and kinematic properties of the jet in the BL Lacertae object OT 081. The multi-frequency VLBI images show that the source consists of a dominant component D and a weak component C1. Our results show a strongly flat spectrum of D, suggesting that it is the core. We derived the equipartition Doppler factors $\delta_{\rm eq}$ of D and C1, which are $\sim$ 32.0 and $\sim$ 2.46, respectively. Moreover, we estimated the variations of Γ from 16 to 20 and ϕ from 0.°68 to 8.°93 by deriving the apparent speed with three VLBI images at 15 GHz. These results show that $\delta_{\rm eq}$ does not strongly depend on the variation of Γ, but the variation of ϕ. We investigated the relation between the radio variability of OT 081 and the variation of ϕ . However, we can not accurately measure the real size and the apparent speed for component D using our VLBI observations. Hence, a higher resolution VLBI observation is necessary to clarify the relation between the variability of the flux density and the variation of ϕ. Therefore, we have already planned an 86-GHz VLBI observation of OT 081, which can achieve an angular resolution of 0.05 mas.

We gratefully acknowledge the VSOP and VLBA Project, which are led by the Institute of Space and Astronautical Science (ISAS) and the National Radio Astronomy Observatory (NRAO), respectively. We are gratefull to Dr. E. Valtaoja, who provided the result of the 22-GHz total flux density (Metsähovi Observatory). This research has made use of the data from the University of Michigan Radio Astronomy Observatory, which is supported by the National Science Foundation and by funds from the University of Michigan.

References

Clements S.D., Smith A.G., Aller H.D., Aller M.F. 1995, AJ 110, 529
Fey A.L., Charlot P. 1997, ApJS 111, 95
Fey A.L., Clegg A.W., Fiedler R.L. 1996a, ApJ 468, 543
Fey A.L., Clegg A.W., Fomalont E.B. 1996b, ApJS 105, 299
Ghisellini G., Padovani P., Celotti A., Maraschi L. 1993, ApJ 407, 65

© Astronomical Society of Japan • Provided by the NASA Astrophysics Data System

2000PASJ...52.1037I

Güijosa A., Daly R.A. 1996, ApJ 461, 600
Hirabayashi H., Hirosawa H., Kobayashi H., Murata Y., Edwards P.G., Fomalont E.B., Fujisawa K., Ichikawa T. et al. 1998, Science 281, 1825
Kellermann K.I., Vermeulen R.C., Zensus J.A., Cohen M.H. 1998, AJ 115, 1295
Lobanov A.P., Krichbaum T.P., Graham D.A., Witzel A., Zensus J.A. 1999, in 2nd millimeter-VLBI science workshop, ed A. Greve, T.P. Krichbaum, (Library IRAM Press, IRAM Granada, Spain), p1
Marscher A.P., 1987, in Superluminal Radio Sources, ed J.A. Zensus, T.J. Pearson (Cambridge Univ. Press, Cambridge), p280
Miller J.S., French H.B., Hawley S.A. 1978, ApJ 219, L85
Napier P.J., Bagri D.S., Clark B.G., Rogers A.E.E., Romney J.D., Thompson A.R., Walker R.C. 1994, Proc. IEEE 82, 658
Pacholczyk A.G. 1970, Radio Astrophysics, W.H. Freeman and Co., San Francisco)
Pearson T.J. 1991, BAAS 23, 991
Readhead A.C.S. 1994, ApJ 426, 51
Reuter H.-P., Kramer C., Sievers A., Paubert G., Moreno R., Greve A., Leon S., Panis J.F. et al. 1997, A&AS 122, 271
Scott M.A., Readhead A.C.S. 1977, MNRAS 180, 539
Shepherd M.C., Pearson T.J., Taylor G.B. 1994, BAAS 26, 987
Teräsranta H., Tornikoski M., Mujunen A., Karlamaa K., Valtonen T., Henelius N., Urpo S., Lainela M. et al. 1998, A&AS 132, 305
Urry C.M., Padovani P. 1995, PASP 107, 803
Urry C.M., Sambruna R.M., Worrall D.M., Kollgaard R.I., Feigelson E.D., Perlman E.S., Stocke J.T. 1996, ApJ 463, 424
Waltman E.B., Fiedler R.L., Johnston K.J., Spencer J.H., Florkowski D.R., Josties F.J., McCarthy D.D., Matsakis D.N. 1991, ApJS 77, 379

© Astronomical Society of Japan • Provided by the NASA Astrophysics Data System